Photochemical Reactions of Cyclohexanone: Mechanisms and Dynamics

Published as part of The Journal of Physical Chemistry A virtual special issue "Mark S. Gordon Festschrift".

Dorit Shemesh,[†] Sergey A. Nizkorodov,[‡] and R. Benny Gerber*[,†,‡]

[†]Institute of Chemistry and The Fritz Haber Research Center, The Hebrew University, Jerusalem 91904, Israel
[‡]Department of Chemistry, University of California, Irvine, California 92697, United States

S *Supporting Information*

ABSTRACT: Photochemistry of carbonyl compounds is of major importance in atmospheric and organic chemistry. The photochemistry of cyclohexanone is studied here using on-the-fly molecular dynamics simulations on a semiempirical multi-reference configuration interaction potential-energy surface to predict the distribution of photoproducts and time scales for their formation. Rich photochemistry is predicted to occur on a picosecond time scale following the photoexcitation of cyclohexanone to the first singlet excited state. The main findings include: (1) Reaction channels found experimentally are confirmed by the theoretical simulations, and a new reaction channel is predicted. (2) The majority (87%) of the reactive trajectories start with a ring opening via C−C$_\alpha$ bond cleavage, supporting observations of previous studies. (3) Mechanistic details, time scales, and yields are predicted for all reaction channels. These benchmark results shed light on the photochemistry of isolated carbonyl compounds in the atmosphere and can be extended in the future to photochemistry of more complex atmospherically relevant carbonyl compounds in both gaseous and condensed-phase environments.
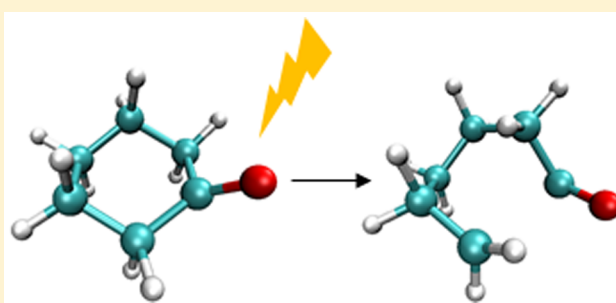
I. INTRODUCTION

The photochemistry of carbonyl compounds is an important topic in organic and atmospheric chemistry.[1−3] Atmospheric carbonyl compounds are directly emitted by combustion sources and are important secondary oxidation products of virtually all hydrocarbons. Carbonyls have a large influence on photochemical smog formation, because they serve as precursors of free radicals, ozone, peroxyacyl nitrates, and particulate matter. Moreover, several carbonyls including formaldehyde, acetaldehyde, and acrolein have also received regulatory attention as toxic air contaminants, mutagens, eye irritants, and carcinogens.[4,5] As a result, there is a large interest in the atmospheric chemistry and photochemistry of these molecules, both when isolated in the gas phase and when embedded in aerosol particles.[6]

Two main types of photochemical reactions observed in aldehydes and ketones include (1) Norrish type I reaction starting with a C−C$_\alpha$ bond cleavage adjacent to the carbonyl group and (2) Norrish type II reaction starting with a γ-H atom transfer to the carbonyl group. The relative yield of these reactions depends strongly on the size of the carbonyl, but other factors such as the structure and bond conjugation in the carbonyl group substituents are important as well.[7]

A number of research groups have experimentally explored the gas-phase photochemistry of small aldehydes, for example (this is not a comprehensive list of references; just representative examples are given), acetaldehyde,[8] propanal,[9] butanal and its derivatives,[10] heptanal,[11] and other small aldehydes.[12] Theoretically, the studies have included calculations on important structures along possible reaction pathways and molecular dynamics simulation on small systems such as formaldehyde and acetaldehyde.[13−16] Our recent study of photochemistry of pentanal clusters suggested that photochemical reactions of aldehydes in gas-phase and in aerosol particles could be very different.[17]

Photochemistry of aliphatic ketones has been thoroughly studied as well.[1−3] Acetone, the simplest ketone, has been studied extensively, and its photochemistry has been considered as representative for larger ketones. Noteworthy is the review on the photochemistry of acetone,[18] as well as more recent experimental and theoretical work on this topic.[19−21] The initial excitation is to the S$_1$ state (nπ* state of the carbonyl group), and it is followed by diverse scenarios such as internal conversion to the ground state and intersystem crossing (ISC) to the triplet state. The yield of each reaction channel depends strongly on the environment (free molecule vs solvated molecule) and on the excitation energy. The main reaction in this case is the cleavage of a C−C$_\alpha$ bond adjacent to the

carbonyl group (Norrish I reaction) on either the ground state or the triplet state resulting in the formation of an acetyl and a methyl radical. Already for this small ketone, the photochemistry is very complex and involves at least three potential-energy surfaces (S_0, S_1, and T_1). In the theoretical treatment so far, a full comprehensive description of the different channels of photochemical reactions has hitherto not been given even for small ketones.

Photochemistry of cyclic ketones has been studied, in part because of the interest in the effect of the ring strain on the mechanisms, for example, in cyclobutanone.[22] Basic knowledge of the reaction products of cyclic ketones was obtained by several research groups and reviewed in the classic photochemistry textbooks.[1,2] The studies so far have revealed mostly the reaction products, with limited details on the detailed molecular mechanism and the time scales of the reactions. In particular, very few theoretical studies focusing on the dynamical evolution after photoexcitation have been published. It is therefore of interest to explore the time-dependent dynamics of different photochemical channels in cyclic ketones—this is the primary objective of this paper.

Photoexcitation of cyclic ketones is believed to start with a cleavage of one of the two C—C_α bonds near the carbonyl group, forming a diradical. Scheme 1 shows a summary of

Scheme 1. Primary Products of Cyclohexanone Photolysis Observed in Previous Experiments[a]
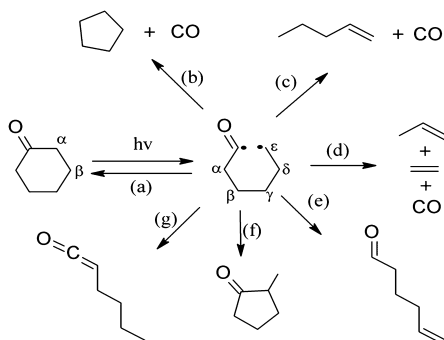
[a]The initial excitation creates a diradical intermediate shown in the middle. The subsequent channels are (a) recombination; (b) decarbonylation accompanied by cyclization into cyclopentane; (c) decarbonylation accompanied by an H-atom transfer to form 1-pentene; (d) decarbonylation accompanied by a disproportionation into propene and ethene; (e) an intramolecular H-atom transfer leading to 5-hexenal; (f) a ring contraction into 1-methyl-cyclopentanone; (g) an intramolecular H-atom transfer leading to 1-hexen-1-one (ketene). Additional processes, which open at higher excitation energies, are not shown.

possible reactions following the initial α-cleavage as reviewed in the literature.[1,2,23−31] The scheme is drawn for cyclohexanone, but similar processes occur in other unstrained cyclic ketones, such as cyclopentanone and cycloheptanone. The disproportionation of the diradical can lead either to two (or more) closed-shell species or to a new cyclic species. However, in the literature, there is no direct evidence, whether the products are indeed formed by a diradical intermediate or by an alternative concerted pathway as suggested by Calvert and Pitts.[1] The present study does support the diradical intermediate mechanism.

This study focuses on the photochemical dynamics of cyclohexanone. This ketone is produced in the atmosphere by

oxidation of cyclohexane by hydroxyl radical (OH); the same reaction is often used to scavenge OH in laboratory experiments.[32] Cyclohexanone and cyclohexane are directly emitted by chemical industry, because they are key precursors to nylon. The structural motif of cyclohexanone is also found in naturally emitted products, such as camphor. The primary atmospheric sink for cyclohexanone is its reaction with OH (k = 6×10^{-12} cm^3 molecule^{-1} s^{-1},[33] resulting in a lifetime of 2 d at [OH] = 1×10^6 molecules cm^{-3}) and photolysis. Similar to other aliphatic ketones, cyclohexanone has an n→π* transition centered at 290 nm with a peak absorption cross section of 4×10^{-20} cm^2 molecule^{-1}.[34] The lifetime of cyclohexanone with respect to photolysis would have been 9 h if it were to photolyze with unity quantum yield (the solar flux for this estimation came from the tropospheric ultraviolet and visible model[35] with a solar zenith angle of zero at sea-level, overhead ozone of 300 Dobson units, and surface albedo of 0.1). However, the photolysis quantum yield is likely to be smaller than unity.[1] Approximating the wavelength-dependent photolysis quantum yield of cyclohexanone by that of acetone[36] increases the lifetime to 190 h under the same conditions. Therefore, photolysis is the second most important mechanism of atmospheric removal of cyclohexanone, and the importance of photolysis relative to OH oxidation increases with altitude, as it does for acetone.[37]

Most previous studies on cyclohexanone aimed at the determination of its structure, for example, by gas-phase electron diffraction including microwave data[38,39] and by theoretical methods using various levels of theory.[40,41] The most relevant experimental studies of photochemistry of cyclohexanone are summarized in Table S1 in the Supporting Information to this article. Carbon monoxide, cyclopentane, and 1-pentene, resulting from the C—C_α bond cleavage (channels b and c in Scheme 1), were identified as major products of photolysis, and ethene + propene + CO (channel d) were identified as minor products of photolysis already in early studies.[23−25] The formation of 5-hexenal (channel e) was observed in 313 nm photolysis in both gas and liquid phase.[26,27] A ring-contraction product 2-methyl-cyclopentane (channel f) was identified in liquid phase photolysis of cyclohexanone.[27] The 1-hexen-1-one ketene product (channel g) was observed in a matrix isolation photolysis of cyclohexanone.[31] Photosensitization experiments relying on excitation of cyclohexanone by triplet states of benzene[28] and mercury atoms[30] showed that both singlet and triplet states of cyclohexanone contributed to the products; for example, 5-hexenal was clearly a product forming on the triplet potential-energy surface.[28] Vacuum UV photolysis accessing the n→σ_{CO}* and n→σ_{CC}* states was performed at much higher energies than considered here, and numerous additional channels, such as the formation of molecular hydrogen, were found.[29,42] The C2 photofragments grew in prominence relative to the C5 photofragments at these high excitation energies. Furthermore, there was evidence for breaking a C_α—C_β bond following the excitation.[29]

The theoretical study performed by Xia and co-workers on excited-state ring-opening mechanism of cyclic ketones predicted an involvement of the T_1 state in the ring-opening mechanism.[43] Their calculations predicted a barrier on the S_1 state along the ring-opening coordinate, which then leads to a conical intersection with the S_0 state. From an energetic point of view, the authors concluded that an ISC to the T_1 state followed by a ring opening is favored. However, ISC is a spin-forbidden process occurring on a time scale of ∼1×10^{-9} s. It is

therefore possible that the reaction will still take place on the S_1 state at higher excitation energies provided that it is faster than the ISC time scale. It is our goal to fully understand the detailed mechanism of the photoexcitation dynamics on the S_1 surface of cyclohexanone.

Theoretical description of the photoexcitation of cyclic ketones requires adequate potential-energy surfaces for all the relevant electronic states. Currently, available knowledge on the potential-energy surfaces involved in the dynamics (singlets or triplets) is very limited. First attempts to explore the potential-energy surfaces involved in the photolysis of cyclohexanone were done in the theoretical work by Xia et al.[43] Their study focused on the first step after photoexcitation, namely, the ring-opening mechanism. They compared the energetic barrier in different cyclic ketones (cyclopropanone to cyclohexanone) for ring opening on the S_1 and T_1 states and concluded that the electronic state involved in the dynamics depends on the identity of the cyclic ketone. Specifically for cyclohexanone the study predicted a barrier of 19.7 kcal/mol on the S_1 state and almost no barrier on the T_1 state for the ring-opening mechanism. The authors concluded that the ring-opening mechanism will be blocked in the S_1 state.

Our main goal is to study the photochemistry of cyclohexanone in its lowest electronically excited S_1 singlet state. The scientific questions promoting our study include:

(1) Do the important photochemical processes take place on the singlet excited state?

(2) What is the predicted product distribution following the photoexcitation of cyclohexanone? How does it compare with the experimental measurements?

(3) What are the time scales and mechanisms for the formation of the products?

In this study, we answer these questions by theoretically modeling the photochemistry of cyclohexanone using on-the-fly molecular dynamics on a semiempirical potential-energy surface.

II. METHODS

The aim here is to provide a comprehensive understanding of the photodissociation dynamics of the cyclohexanone system. Two aspects are therefore of key importance in the simulation approach: the choice of an appropriate potential and the level and type of the dynamical description of the system.

We first discuss the choice of the *potential*. Very accurate potentials exist for treating excited states, such as CASPT2,[44] TD-DFT,[45] MRCI,[46] etc. However, such potentials are computationally expensive, especially in combination with dynamics, where the calculation of the potential-energy surface is repeated millions of times for each time step during the simulation. On the basis of our previous studies on the photochemistry of carbonyl compounds, we employed the **o**rthogonalization-**c**orrected **m**ethod **2** (OM2) potential[47] for the ground state calculations and **o**rthogonalization-**c**orrected **m**ethod **2**/**m**ultireference **c**onfiguration **i**nteraction (OM2/MRCI) potentials for the description of the excited states.[48] The semiempirical potential-energy surfaces employed here have been proven to be reliable and of sufficient accuracy for modeling molecules and processes of the type studied in this work.[17,49−53] We note that for the method used here, the forces can be computed directly (analytic gradients are available), which is advantageous for an efficient propagation of the dynamics. Additionally, the method permits long time scale simulations, up to 100 ps in our case.

The second challenge is the theoretical description of the excited state *dynamics*. Several methods (and their implementation into different programs) exist that address this aim.[54−63] The choice of the method depends on the complexity of the dynamical evolution, that is, whether state-switching between the same or different spin states (singlet or triplet) is allowed. Noteworthy is the recent development of the Surface Hopping including Arbitrary Couplings (SHARC) software suite,[62,64,65] which enables dynamical treatment of surface hopping between the singlet and triplet states. In a recent study, the deactivation mechanism of 2-thiouracil was performed with this program using a CASPT2 potential-energy surface.[66] Currently, because of the high computational cost, the simulation time scale is very limited (1 ps in the cited study), which is more than 2 orders of magnitude shorter than that afforded by the OM2/MRCI method.

In the simulations reported here, the dynamics was pursued solely on the S_1 surface. Classical trajectories were computed on-the-fly on the OM2/MRCI semiempirical potential.[48] Despite the fact that photochemistry of carbonyls is expected to involve both the S_1 and T_1 excited states, the large number of reactive trajectories proves that at least some of the reactions are indeed taking place on the S_1 state. The longer the time scale for a given channel, the greater is the likelihood that it will be affected by singlet-to-triplet ISC transition. In general, ISC to the triplet state is possible, and reactions might be energetically more favorable on the triplet state, as described in ref 43. The location of the triplet state in cyclohexanone is ∼1 eV below the S_1 state, which makes the ISC theoretically possible. However, the ISC time scales are believed to be $\sim 1 \times 10^{-9}$ s. The reactions simulated here occur within 100 ps, much faster than the expected ISC time scales. We therefore believe that the ISC followed by the triplet-state dynamics is not the dominant pathway for this system. We plan a more rigorous approach treating both singlet and triplet electronic state dynamics of this and similar systems in the near future.

Ground-state minima were calculated and compared to the literature values. The structures were optimized with the high-level MP2 method in conjunction with the resolution of identity (RI) approximation[67] using cc-pVDZ as the basis set.[68] The OM2/MRCI method was then applied to these structures, and geometrical and energetic properties were compared. The active space was chosen to include the highest five occupied and the lowest five unoccupied orbitals. Three reference configurations were used for the MRCI calculations, namely, closed-shell, singly excited, and doubly excited configurations. Electronic excitation energies of the global minimum structure were calculated with the same methodology. The ab initio method ADC(2)[69] was used for validation of the excited-state properties of the semiempirical method.

Sampling of the initial conditions was performed by running molecular dynamics simulation for 10 ps with a time step of 0.1 fs at 300 K using OM2 for the electronic ground state. Structures were chosen such that the excitation energy of the selected configuration to the first excited singlet state lies in the range of ±0.5 eV of the S_1 excitation of the global minimum. Since the structure varies along the molecular dynamics simulation on the ground state, the first excited-state energy varies as well. We therefore believe that the range of ±0.5 eV is reasonable for considering geometries around the global minimum. The S_2 state lies ∼3 eV above the S_1 state and is

therefore not considered relevant in range of the excitation energy. The chosen structures were used as starting configuration on the S_1 surface, resulting in a total number of 122 trajectories. The simulations were run for up to 100 ps with a time step of 0.1 fs. The small time-steps used here in both ground- and excited-state simulations were needed because the electronic states were found to depend quite strongly on the nuclear positions, especially for S_1. Forty-six trajectories were aborted earlier due to problems related to sudden energy jumps (violation of energy conservation) because of orbital switching described in more detail in ref 70. Those trajectories were disregarded. Six trajectories were unreactive, in a sense that they produced no reactions at the end of the simulation time. The number of trajectories employed here enables us to predict relatively minor reactions, which have a probability of ~1−2% (that is, one trajectory of the 76 successfully completed trajectories).

III. RESULTS AND DISCUSSION

a. Initial Structure. The initial minimal-energy structure of cyclohexanone (Figure 1) corresponds to a chair conformer
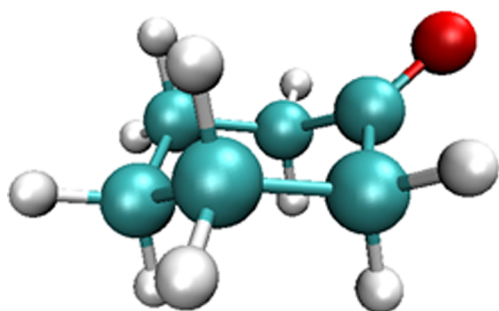

Figure 1. Optimized chair conformer of cyclohexanone, corresponding to the global energy minimum for the system. Atom colors: H−gray, C−turquoise, O−red.

with a planar C−C(=O)−C part as reported in refs 38, 39, and 41 and as predicted by both MP2 and OM2 methods in this work. Gas-phase electron diffraction and microwave data[38,39] observed only the chair conformer; no evidence for the boat conformer was found in these studies. However, it was observed by NMR spectroscopy[71−73] that cyclohexanone can interconvert from one chair conformer to another chair conformer in solution. Theoretical calculations predicted three stable minima with possible interconversion pathways between them. However, the energy for the higher-lying conformers was calculated to be at least 3.10 kcal/mol (0.13 eV) depending on the level of theory, making them unimportant for the room-temperature dynamics.

For example, MP2 calculations predict the twist-boat conformer to be 0.197 eV higher than the chair conformer, corresponding to a Boltzmann factor of 0.05% at 300 K for the twist-boat conformer. With a somewhat lower energy of 0.13

eV predicted by the theoretical and experimental finding of refs 71−73, the population of the higher-energy conformer is still negligible (0.6%).

Cyclohexanone can adopt both keto and enol structures. However, MP2 calculations for the enol form of cyclohexanone predict this structure to be 0.65 eV higher in energy than the global minimum. Therefore, the enol form can be neglected for these room-temperature simulations.

To conclude, our findings support the fact that only the chair conformer of the keto form of cyclohexanone is relevant for the room-temperature photochemistry of this system.

b. Excited-State Energies. Table 1 provides the vertical excitation energies as computed with ADC(2)/cc-pVDZ. The ground-state dipole for this structure is 3.35 D.

The first excited state is an n→π* transition located on the carbonyl group. This excitation represents the typical excitation of the carbonyl chromophore. The predicted excitation energy is 4.19 eV. The experimental value, which corresponds to the peak of the n→π* band at 290 nm, is 4.3 eV. The excited-state energy is only slightly underestimated compared to the experimental value. The second excited state is theoretically predicated at much higher energy (7.68 eV) and therefore is not accessible at excitation wavelengths of relevance to tropospheric photochemistry. The first excited state has an oscillator strength of zero for the minimal energy structure, in agreement with the symmetry-forbidden nature of this transition. However, the state can still be photochemically accessed from the nonequilibrium structures excited by thermal fluctuations, which break the molecular symmetry.

For comparison, Table 2 shows the OM2/MRCI vertical excitation energies. Clearly, the first excited state is described very similarly, with an excitation energy of 3.94 eV, ~0.25 eV less than predicted by ADC(2). The next two excited states are much higher in energy, similar to the ADC(2) case. Because of the large energy gap between the S_1 and the S_2 states, the S_2 and higher states should be irrelevant for the excited-state dynamics at the relatively small excitation energies used in this work.

The Supporting Information (Tables S2 and S3) provides vertical excitation energies of the twist-boat conformer with the ADC(2) and OM2/MRCI methods, as an additional validation of the OM2/MRCI method. The results are similar to the chair conformer, and it can therefore be concluded that the OM2/MRCI method is of sufficient accuracy for treating the photodissociation dynamics of this system.

c. Photoexcitation Dynamics on the S_1 State. Figure 2 summarizes the main events observed in the dynamics, and Table S4 lists the actual numbers of the corresponding trajectories. Important reaction channels are discussed below in more detail. Most of the channels start with the C−C_α bond cleavage, in agreement with the previous literature on photochemistry of cyclohexanone. Upon excitation to the S_1 state, the C=O bond is weakened, and the carbon atom

Table 1. ADC(2) Vertical Excitation Energies for the Global Minimum (Chair Conformer) of Cyclohexanone

state	energy (in eV)	orbital transition[a]	description	oscillator strength	dipole moment (debye)
1	4.19	HOMO → LUMO 63%	n(oxygen) → π*(C=O)	0.0000	0.79
2	7.68	HOMO → LUMO+2 55%	n(oxygen) → π*(C=O)	0.0084	4.98
3	8.22	HOMO → LUMO+1 73%		0.0012	5.36

[a]The percentage refers to the fractional weight of the dominant excited state wavefunction in this transition.

Table 2. OM2/MRCI Vertical Excitation Energies for the Global Minimum (Chair Conformer) of Cyclohexanone

| state	energy (in eV)	orbital transition	description	oscillator strength	dipole moment (debye)
1	3.94	HOMO → LUMO 90%	n(oxygen) → π^*(C=O)	0.0008	2.84
2	6.59	HOMO → LUMO+1 92%		0.3391	1.43
3	7.35	HOMO−1 → LUMO 96%		0.1791	10.26
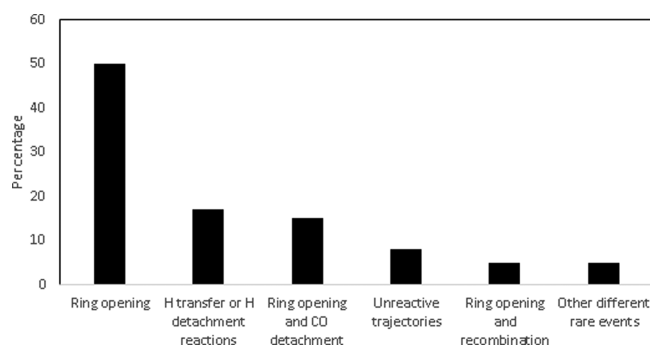
Figure 2. Percent fraction of different reaction channels observed in the dynamics following excitation to the S_1 state.

attached to the carbonyl oxygen adopts a pyramidal configuration.

The major type of reaction is the ring-opening channel, observed in ~50% of the trajectories. Approximately 17% of the trajectories show either a H atom transfer or H atom detachment combined with additional steps before or after, specifically: ring opening followed by an H atom transfer; H atom detachment; H atom transfer and HCO detachment; H atom transfer and further fragmentation. Approximately 15% of the trajectories show ring opening and CO detachment. Minor contributions to the photodissociation dynamics came from unreactive trajectories and from trajectories where the ring opening was followed by recombination. Rare events are reported in Figure 2 as well. All of these reactions are described in more detail and compared to Scheme 1 below.

c.1. C−C_α Cleavage (Ring Opening). A large fraction (50%) of the trajectories resulted in ring opening via C−C_α cleavage creating a diradical that survived until the end of the simulation. Another 30% of the trajectories produced ring opening followed by additional steps. This means that as many as 80% **of all the trajectories** resulted in the initial C−C_α cleavage, supporting the expectation that the diradical formation should be the primary step after excitation.[2] The average time scale for the cleavage was 14.5 ps. Representative snapshots for a trajectory showing this reaction channel are depicted in Figure 3.

c.2. C−C_α Cleavage (Ring Opening) Followed by Recombination. Four trajectories (5%) resulted in the ring opening followed by recombination (as opposed to the
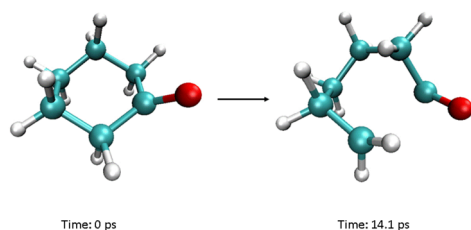
Figure 3. Snapshots of a trajectory showing ring opening via C−C_α cleavage.

previously considered case where the diradical survived until the end of the simulation). The average time scale for the ring-opening event was ~13 ps, with the recombination occurring at ~25 ps. This process corresponds to the reaction (a) in Scheme 1.

c.3. C−C_α Cleavage (Ring Opening) Followed by CO Detachment. In this reaction channel, the initial ring opening is followed by a CO detachment, resulting in pentane-1,5-diyl as the intermediate product. Approximately 15% of the trajectories resulted in this reaction. Snapshots of this process are shown in Figure 4. The pentane-1,5-diyl diradical is not
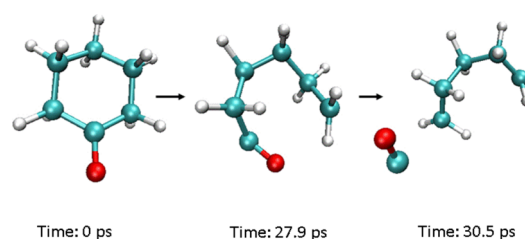

Figure 4. Snapshots of a trajectory showing ring opening followed by CO detachment.

expected to be stable and can be expected to react further as described in Scheme 1 reactions (b) and (c), resulting in cyclopentane and 1-pentene, respectively.

The average time scale for the ring opening in these trajectories was 32 ps. The average time scale for the expulsion of CO was 35 ps. One of the trajectories had the two steps occurring nearly simultaneously, that is, the cleavage of both of the C−C_α bonds and the CO detachment occurred within one simulation time step. Three trajectories showed additional events after the CO detachment: one corresponding to an H atom transfer, another corresponding to an H atom detachment, and the third one resulting in the pentane-1,5-diyl ring closure to form cyclopentane. The ring closure event is depicted in Figure 5.

The ring closure shown in Figure 5 corresponds to reaction channel (b) in Scheme 1. The H atom transfer we observe is from the middle carbon of pentane-1,5-diyl to the terminal carbon, resulting in pentane-1,3-diyl, which is different from the expected H atom transfer described in channel (c) of Scheme 1. From a mechanistic point of view, the products in reaction channel (c) were not obtained in our simulation by ring opening, CO detachment, and H transfer. Below, an alternative mechanism leading to the products of channel (c) is described in detail, and it consists of the same steps (ring opening, H atom transfer, and CO detachment) but occurring in a different order.

c.4. C−C_α Cleavage (Ring Opening), H Atom Transfer from C_δ to C. Four trajectories (5%) resulted in the C−C_α cleavage followed by an H atom transfer from the C_δ to C atom (the atom labels are shown in Scheme 1 and Figure 6). This transfer converted the diradical into 5-hexenal, as shown in Figure 6. This reaction channel corresponds to the disproportionation described as channel (e) of Scheme 1.
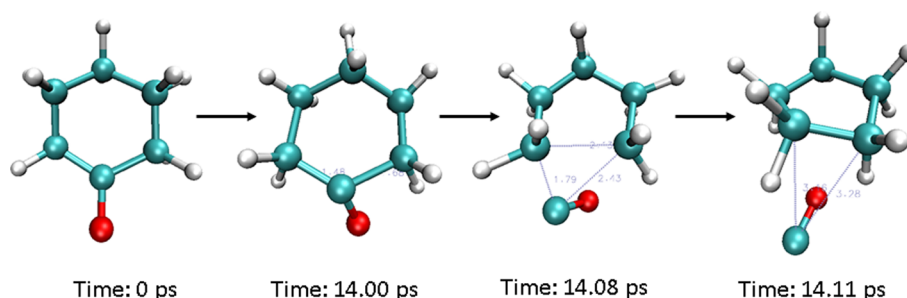
Figure 5. Snapshots of a trajectory showing ring opening, CO detachment, and ring closure.
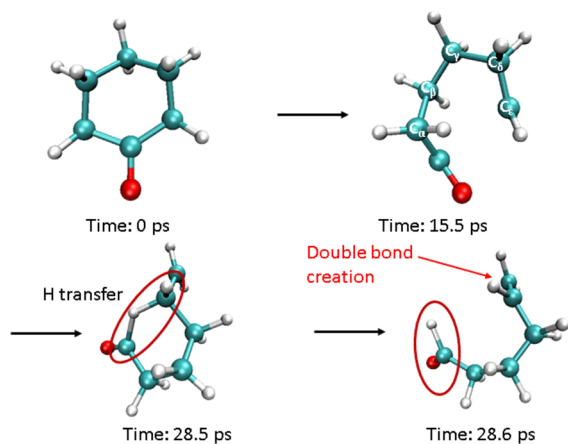

Figure 6. Snapshots of a trajectory showing ring opening followed by an H atom transfer from C_δ to the carbonyl C. The final product is 5-hexenal.

The C_δ–C_ε bond distance changes during this process are depicted in Figure 7. The bond length in the diradical is already
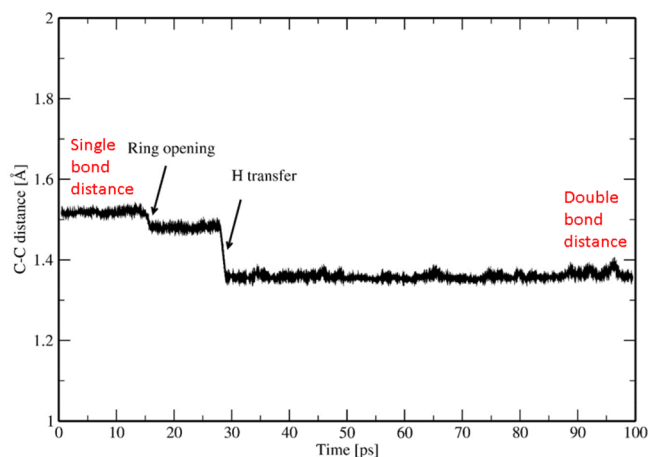
Figure 7. Bond-length variation of the terminal C_δ–C_ε bond along the trajectory depicted in Figure 6.

shortened slightly after the C–C_α cleavage. The H atom transfer creates the double bond by combining the electrons from the diradical located on nearby carbon atoms. The average time scale for ring opening is 13 ps, and the H atom transfer occurs on average at 24 ps.

c.5. C–C_α Cleavage (Ring Opening), H Atom Transfer from C_α to Terminal C_ε. In these four trajectories (5% of all trajectories) the first step is once again the C–C_α cleavage (ring opening). The second step involves an H atom transfer from

C_α to the terminal C_ε in the diradical. Both steps are illustrated in Figure 8a. The H atom transfer leads to a formation of a

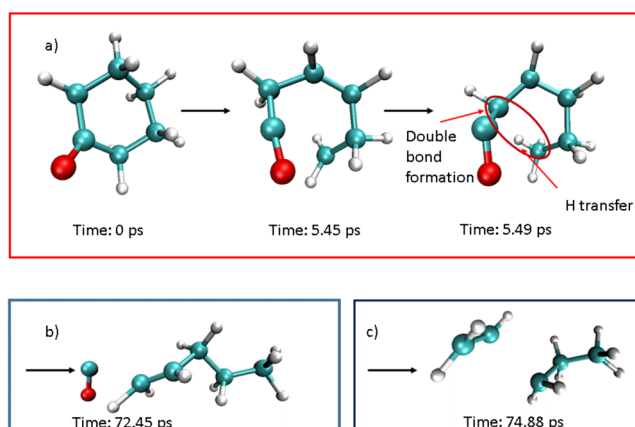**Figure 8.** (a) Ring opening followed by an H atom transfer from C_α to terminal C_ε as seen in four trajectories. (b) Two trajectories show the additional CO detachment. (c) One of these two trajectories shows an additional C–C cleavage after the CO detachment. Times are given for the trajectory showing all the steps.

double bond between two nearby carbons, thereby eliminating the diradical and creating a closed-shell system. This reaction channel is also depicted in Scheme 1, namely, reaction (g) leading to the ketene product. In our simulation two trajectories show an additional step after the ketene formation, namely, the CO detachment shown in Figure 8b. In one of these two trajectories the larger fragment is cleaved into two smaller fragments, corresponding to *n*-propyl and vinyl radicals (Figure 8c). This could eventually lead to the propene and ethene products shown in channel (d) of Scheme 1. The ring opening is observed in an average time of 8.3 ps, the H atom transfer quickly follows at 9.4 ps. The trajectory that shows all four steps is depicted in Figure 8.

c.6. H atom Detachment from C_β. Three trajectories (i.e., 4% of the total trajectories) resulted in an H atom detachment from one of the two C_β atoms in cyclohexanone, without the C–C_α bond cleavage. Because of the symmetry in the molecule, there are four structurally identical H atoms that can be detached. The average time scale for the H atom detachment was 33 ps. This reaction channel has not been previously described in the literature. If it occurs in an oxygen-containing environment, it would give rise to cyclohexanone substituted by either a keto or hydroxyl group in the C_β position; these products have not been observed in previous experiments.

c.7. HCO Detachment and Five-Membered Ring Creation. One interesting reaction trajectory, arguably a rare event,
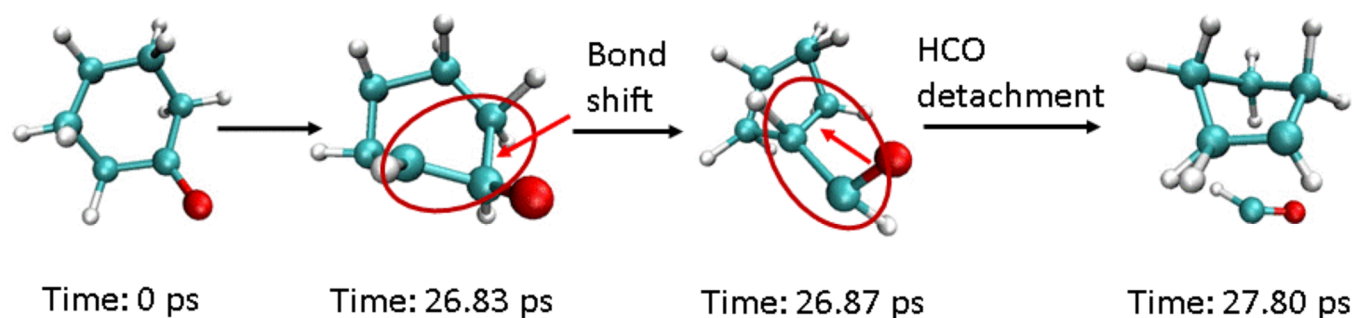
Figure 9. Trajectory showing the creation of a cyclopentyl radical and an HCO radical.

showed the creation of a cyclopentyl radical and an HCO radical. The mechanism is depicted in Figure 9.

At 26.83 ps the bond is shifted such that the ring is shortened from a six-membered carbon ring to a five-membered carbon ring. As a result, the HCO group is now attached loosely to the ring, and after less than 1 ps, the HCO is detached from the system.

IV. SIGNIFICANCE OF RESULTS

Molecular dynamics simulation using the semiempirical OM2/MRCI method was employed in the study of the photo-excitation of cyclohexanone to the first excited singlet state. This study has succeeded in predicting all but one of the six main reaction channels found by previous experiments (Scheme 1 and Table S1). The ring contraction (f), which was not predicted in this work, was only observed in solution[27] and could be specific to the condensed-phase environment or to triplet states of cyclohexanone. The excellent agreement with the experimental observations is a major achievement from a methodological point of view. The semiempirical method used here is both computationally efficient and accurate in describing correctly the potential-energy surface employed due to proper parametrization. In addition to predicting the products, the molecular dynamics simulation has provided mechanistic details and time scales of each process, which were not known so far. Additionally, estimated yields for each process, including rare events, have been calculated.

Specifically, ∼92% of the trajectories were predicted to be reactive. Most of the reactions (∼87% of the reactive trajectories, that is, 80% of the total number of trajectories) started with the ring opening via $C-C_\alpha$ cleavage supporting the assumption of the key role of the diradical shown in Scheme 1. The second step, which occurred in 15% of the trajectories, was the CO detachment. The CO detachment occurred by three different mechanisms in our simulations. In the first mechanism, the ring was cleaved first and was followed by the CO detachment, leaving pentane-1,5-diyl as a fragment. The second mechanism featured the CO detachment as a concerted step, in which simultaneously the ring was opened, the CO molecule detached, and the ring was closed again, resulting in cyclopentane as a product. Finally the third mechanism started from the ring opening, followed by an H atom transfer to form a ketene intermediate, from which CO detached. In all these mechanisms CO was produced with a different coproduct.

Several trajectories predicted hitherto unknown reaction channels. One of them is an H atom detachment from the C_β atom of cyclohexanone. Another is the formation of HCO radical and cyclopentyl radical. These new predictions will be useful in interpreting photochemical pathways in cyclo-hexanone and other cyclic ketones in future experiments.

These reactions appear to take place on an ultrafast time scale, much faster than the likely time scale for the ISC from the singlet to the triplet state. Even the formation of 5-hexenal, which was previously attributed to the triplet excitation of cyclohexanone, was found to occur in under 100 ps in our simulations. This encourages the view that reactions in the singlet state are the dominant ones for this system. Reactions with longer time scales ($t \gg 100$ ps) are more likely to be affected by the $S_1 \rightarrow T_1$ ISC transitions, which are neglected in this paper. In principle, since ∼8% of the reactions were unreactive, those trajectories could theoretically switch on a much longer time scale to the nearby triplet state. We have not explored this possibility because the time needed to simulate the ISC event would be too long for feasible computation time. Additionally the scope of this paper was to demonstrate the ultrafast reactions on the first excited singlet state. Thus, triplet-state dynamics cannot be entirely excluded based on these simulations, and could, for example, be responsible for the ring-contraction process (f) that did not occur in these singlet-state simulations. The success in describing all the important reactions after photoexcitation of cyclohexanone encourages further investigation of related and more complex systems. Such systems might include larger aldehydes and ketones but also carbonyl compounds embedded in a condensed-phase environment. Reactions in a cluster (not considered here) are likely to enhance certain channels, especially ring closure by recombination or further reaction of the diradical with the matrix after initial ring opening. This study opens the field for the study of the photochemistry of aerosols on an atomistic level.

■ ASSOCIATED CONTENT

ⓢ Supporting Information

The Supporting Information is available free of charge on the ACS Publications website at DOI: 10.1021/acs.jpca.6b06184.

> All relevant experimental studies of gas-phase photo-chemistry of cyclohexanone, with their reaction channels and quoted yields; validation of the OM2/MRCI method; statistics of all theoretically predicted reaction channels. (PDF)

■ AUTHOR INFORMATION

Corresponding Author

*E-mail: benny@fh.huji.ac.il. Phone: 972 2 6585732.

Notes

The authors declare no competing financial interest.

REFERENCES

(1) Calvert, J. G.; Pitts, J. N. *Photochemistry;* John Wiley: New York, 1966.

(2) Turro, N. J. *Modern Molecular Photochemistry;* University Science Books: Sausalito, CA, 1991.

(3) Michel, J.; Bonačić-Koutecký, V. *Electronic Aspects of Organic Photochemistry;* Wiley-Interscience: New York, 1990.

(4) Shepson, P. B.; Kleindienst, T. E.; Edney, E. O.; Nero, C. M.; Cupitt, L. T.; Claxton, L. D. Acetaldehyde - the Mutagenic Activity of its Photooxidation Products. *Environ. Sci. Technol.* **1986**, *20*, 1008−1013.

(5) Grosjean, E.; Grosjean, D.; Fraser, M. P.; Cass, G. R. Air Quality Model Evaluation Data for Organics. 2. C-1-C-14 Carbonyls in Los Angeles Air. *Environ. Sci. Technol.* **1996**, *30*, 2687−2703.

(6) George, C.; Ammann, M.; D'Anna, B.; Donaldson, D. J.; Nizkorodov, S. A. Heterogeneous Photochemistry in the Atmosphere. *Chem. Rev.* **2015**, *115*, 4218−4258.

(7) Kletskii, M. E.; Lisovin, A. V.; Burov, O. N.; Kurbatov, S. V. Competing Mechanisms of Norrish and Norrish-like Reactions in a Wide Range of Systems - From Carbonyl Compounds to Nitrogen Oxide Donators. *Comput. Theor. Chem.* **2014**, *1047*, 55−66.

(8) Heazlewood, B. R.; Maccarone, A. T.; Andrews, D. U.; Osborn, D. L.; Harding, L. B.; Klippenstein, S. J.; Jordan, M. J. T.; Kable, S. H. Near-threshold H/D Exchange in CD_3CHO Photodissociation. *Nat. Chem.* **2011**, *3*, 443−448.

(9) Metha, G. F.; Terentis, A. C.; Kable, S. H. Near Threshold Photochemistry of Propanal. Barrier Height, Transition State Structure, and Product State Distributions for the HCO Channel. *J. Phys. Chem. A* **2002**, *106*, 5817−5827.

(10) Tadic, J. M.; Moortgat, G. K.; Bera, P. P.; Loewenstein, M.; Yates, E. L.; Lee, T. J. Photochemistry and Photophysics of n-Butanal, 3-Methylbutanal, and 3,3-Dimethylbutanal: Experimental and Theoretical Study. *J. Phys. Chem. A* **2012**, *116*, 5830−5839.

(11) Paulson, S. E.; Liu, D. L.; Orzechowska, G. E.; Campos, L. M.; Houk, K. N. Photolysis of Heptanal. *J. Org. Chem.* **2006**, *71*, 6403−6408.

(12) Zhu, L.; Tang, Y. X.; Chen, Y. Q.; Cronin, T. Wavelength-Dependent Photolysis of C3-C7 Aldehydes in the 280−330nm Region. *Spectrosc. Lett.* **2009**, *42*, 467−478.

(13) Fang, W. H. Ab Initio Determination of Dark Structures in Radiationless Transitions for Aromatic Carbonyl Compounds. *Acc. Chem. Res.* **2008**, *41*, 452−457.

(14) Fu, B. N.; Shepler, B. C.; Bowman, J. M. Three-State Trajectory Surface Hopping Studies of the Photodissociation Dynamics of Formaldehyde on ab Initio Potential Energy Surfaces. *J. Am. Chem. Soc.* **2011**, *133*, 7957−7968.

(15) Kurosaki, Y. Hydrogen-atom Production Channels of Acetaldehyde Photodissociation: Direct DFT Molecular Dynamics Study. *J. Mol. Struct.: THEOCHEM* **2008**, *850*, 9−16.

(16) Townsend, D.; Lahankar, S. A.; Lee, S. K.; Chambreau, S. D.; Suits, A. G.; Zhang, X.; Rheinecker, J.; Harding, L. B.; Bowman, J. M. The Roaming Atom: Straying from the Reaction Path in Formaldehyde Decomposition. *Science* **2004**, *306*, 1158−1161.

(17) Shemesh, D.; Blair, S. L.; Nizkorodov, S. A.; Gerber, R. B. Photochemistry of Aldehyde Clusters: Cross-molecular Versus Unimolecular Reaction Dynamics. *Phys. Chem. Chem. Phys.* **2014**, *16*, 23861−23868.

(18) Haas, Y. Photochemical Alpha-cleavage of Ketones: Revisiting Acetone. *Photoch Photobio Sci.* **2004**, *3*, 6−16.

(19) Maeda, S.; Ohno, K.; Morokuma, K. A Theoretical Study on the Photodissociation of Acetone: Insight into the Slow Intersystem Crossing and Exploration of Nonadiabatic Pathways to the Ground State. *J. Phys. Chem. Lett.* **2010**, *1*, 1841−1845.

(20) Favero, L.; Granucci, G.; Persico, M. Dynamics of Acetone Photodissociation: a Surface Hopping Study. *Phys. Chem. Chem. Phys.* **2013**, *15*, 20651−20661.

(21) Brogaard, R. Y.; Solling, T. I.; Moller, K. B. Initial Dynamics of the Norrish Type I Reaction in Acetone: Probing Wave Packet Motion. *J. Phys. Chem. A* **2011**, *115*, 556−561.

(22) Lee, N. E.; Lee, E. K. C. Tracer Study of Photochemically Excited Cyclobutanone-2-T and Cyclobutanone. II. Detailed Mechanism Energetics Unimolecular Decomposition Rates and Intermolecular Vibrational Energy Transfer. *J. Chem. Phys.* **1969**, *50*, 2094−2107.

(23) Bamford, C. H.; Norrish, R. G. W. 287. Primary Photochemical Reactions. Part X. The Photolysis of Cyclic Ketones in the Gas Phase. *J. Chem. Soc.* **1938**, 1521−1531.

(24) Benson, S. W.; Kistiakowsky. The Photochemical Decomposition of Cyclic Ketones. *J. Am. Chem. Soc.* **1942**, *64*, 80−86.

(25) Blacet, F. E.; Miller, A. The Photochemical Decomposition of Cyclohexanone, Cyclopentanone and Cyclobutanone. *J. Am. Chem. Soc.* **1957**, *79*, 4327−4329.

(26) Srinivasan, R. Photoisomerization Processes in Cyclic Ketones. II. Cyclohexanone and 2-Methylcyclohexanone. *J. Am. Chem. Soc.* **1959**, *81*, 2601−2604.

(27) Srinivasan, R.; Cremer, S. E. A Photoisomerization Reaction of Cyclic Ketones in Liquid Phase. *J. Am. Chem. Soc.* **1965**, *87*, 1647−1651.

(28) Shortridge, R. G.; Lee, E. K. C. Benzene Photosensitization and Direct Photolysis of Cyclohexanone and Cyclohexanone-2-T in Gas Phase. *J. Am. Chem. Soc.* **1970**, *92*, 2228−2236.

(29) Shortridge, R. G.; Lee, E. K. C. Photochemistry of Cyclohexanone. II. Second and Third Singlet Excited-States. *J. Phys. Chem.* **1973**, *77*, 1936−1943.

(30) Baulch, D. L.; Colburn, A.; Lenney, P. W.; Montague, D. C. Hg(63p1) Photosensitization of Cyclohexanone - Role of Triplet Biradical Intermediates. *J. Chem. Soc., Faraday Trans. 1* **1981**, *77*, 1803−1812.

(31) Hoops, M. D.; Ault, B. S. Matrix Isolation Study of the Photochemical Reaction of Cyclohexane, Cyclohexene, and Cyclopropane with Ozone. *J. Mol. Struct.* **2009**, *929*, 22−31.

(32) Atkinson, R.; Aschmann, S. M.; Arey, J.; Shorees, B. Formation of OH Radicals in the Gas-Phase Reactions of O_3 with a Series of Terpenes. *J. Geophys. Res.* **1992**, *97*, 6065−6073.

(33) Dagaut, P.; Wallington, T. J.; Liu, R. Z.; Kurylo, M. J. A Kinetics Investigation of the Gas-Phase Reactions of OH Radicals with Cyclic-Ketones and Diones - Mechanistic Insights. *J. Phys. Chem.* **1988**, *92*, 4375−4377.

(34) Iwasaki, E.; Matsumi, Y.; Takahashi, K.; Wallington, T. J.; Hurley, M. D.; Orlando, J. J.; Kaiser, E. W.; Calvert, J. G. Atmospheric Chemistry of Cyclohexanone: UV Spectrum and Kinetics of Reaction with Chlorine Atoms. *Int. J. Chem. Kinet.* **2008**, *40*, 223−229.

(35) Madronich, S. *Ultraviolet and Visible (TUV) Radiation Model.* https://www2.acom.ucar.edu/modeling/tropospheric-ultraviolet-and-visible-tuv-radiation-model accessed May 21.

(36) Sander, S. P.; et al. *Chemical Kinetics and Photochemical Data for Use in Atmospheric Studies,* Evaluation No. 17. JPL Publication 10-6; NASA Jet Propulsion Laboratory: Pasadena, CA, 2011.

(37) Blitz, M. A.; Heard, D. E.; Pilling, M. J.; Arnold, S. R.; Chipperfield, M. P. Pressure and Temperature-dependent Quantum Yields for the Photodissociation of Acetone between 279 and 327.5 nm. *Geophys. Res. Lett.* **2004**, *31*, L06111.

(38) Dillen, J.; Geise, H. J. The Molecular-Structure of Cyclohexanone Determined by Gas-Phase Electron-Diffraction, Including Microwave Data. *J. Mol. Struct.* **1980**, *69*, 137−144.

(39) Alonso, J. L. Microwave-Spectrum of Cyclohexanone. *J. Mol. Struct.* **1981**, *73*, 63−69.

(40) Langley, C. H.; Lii, J. H.; Allinger, N. L. Molecular Mechanics Calculations on Carbonyl Compounds. III. Cycloketones. *J. Comput. Chem.* **2001**, *22*, 1451−1475.

(41) Devlin, F. J.; Stephens, P. J. Ab Initio Density Functional Theory Study of the Structure and Vibrational Spectra of Cyclohexanone and its Isotopomers. *J. Phys. Chem. A* **1999**, *103*, 527−538.

(42) Scala, A. A.; Ballan, D. G. Vacuum Ultraviolet Photolysis of Cyclohexanone. *J. Phys. Chem.* **1972**, *76*, 615−620.

(43) Xia, S. H.; Liu, X. Y.; Fang, Q.; Cui, G. L. Excited-State Ring-Opening Mechanism of Cyclic Ketones: A MS-CASPT2//CASSCF Study. *J. Phys. Chem. A* **2015**, *119*, 3569−3576.

(44) Roos, B. O.; Linse, P.; Siegbahn, P. E. M.; Blomberg, M. R. A. A Simple Method for the Evaluation of the 2nd-Order Perturbation Energy from External Double-Excitations with a CASSCF Reference Wavefunction. *Chem. Phys.* **1982**, *66*, 197−207.

(45) Runge, E.; Gross, E. K. U. Density-Functional Theory for Time-Dependent Systems. *Phys. Rev. Lett.* **1984**, *52*, 997−1000.

(46) Werner, H. J.; Knowles, P. J. An Efficient Internally Contracted Multiconfiguration Reference Configuration-Interaction Method. *J. Chem. Phys.* **1988**, *89*, 5803−5814.

(47) Weber, W.; Thiel, W. Orthogonalization Corrections for Semiempirical Methods. *Theor. Chem. Acc.* **2000**, *103*, 495−506.

(48) Koslowski, A.; Beck, M. E.; Thiel, W. Implementation of a General Multireference Configuration Interaction Procedure with Analytic Gradients in a Semiempirical Context using the Graphical Unitary Group Approach. *J. Comput. Chem.* **2003**, *24*, 714−726.

(49) Epstein, S. A.; Shemesh, D.; Tran, V. T.; Nizkorodov, S. A.; Gerber, R. B. Absorption Spectra and Photolysis of Methyl Peroxide in Liquid and Frozen Water. *J. Phys. Chem. A* **2012**, *116*, 6068−6077.

(50) Lignell, H.; Epstein, S. A.; Marvin, M. R.; Shemesh, D.; Gerber, R. B.; Nizkorodov, S. A. Experimental and Theoretical Study of Aqueous cis-Pinonic Acid Photolysis. *J. Phys. Chem. A* **2013**, *117*, 12930−12945.

(51) Romonosky, D. E.; Nguyen, L. Q.; Shemesh, D.; Nguyen, T. B.; Epstein, S. A.; Martin, D. B. C.; Vanderwal, C. D.; Gerber, R. B.; Nizkorodov, S. A. Absorption Spectra and Aqueous Photochemistry of Beta-hydroxyalkyl Nitrates of Atmospheric Interest. *Mol. Phys.* **2015**, *113*, 2179−2190.

(52) Shemesh, D.; Gerber, R. B. Femtosecond Timescale Deactivation of Electronically Excited Peroxides at Ice Surfaces. *Mol. Phys.* **2012**, *110*, 605−617.

(53) Shemesh, D.; Lan, Z. G.; Gerber, R. B. Dynamics of Triplet-State Photochemistry of Pentanal: Mechanisms of Norrish I, Norrish II, and H Abstraction Reactions. *J. Phys. Chem. A* **2013**, *117*, 11711−11724.

(54) Ben-Nun, M.; Quenneville, J.; Martinez, T. J. Ab Initio Multiple Spawning: Photochemistry from First Principles Quantum Molecular Dynamics. *J. Phys. Chem. A* **2000**, *104*, 5161−5175.

(55) Batista, V. S.; Coker, D. F. Nonadiabatic Molecular Dynamics Simulation of Photodissociation and Geminate Recombination of I-2 Liquid Xenon. *J. Chem. Phys.* **1996**, *105*, 4033−4054.

(56) Bernard, Y. A.; Shao, Y. H.; Krylov, A. I. General Formulation of Spin-flip Time-dependent Density Functional Theory using Non-collinear Kernels: Theory, Implementation, and Benchmarks. *J. Chem. Phys.* **2012**, *136*, 204103.

(57) Doltsinis, N. L.; Marx, D. Nonadiabatic Car-Parrinello Molecular Dynamics. *Phys. Rev. Lett.* **2002**, *88*, 166402.

(58) Domcke, W.; Yarkony, D. R. Role of Conical Intersections in Molecular Spectroscopy and Photoinduced Chemical Dynamics. *Annu. Rev. Phys. Chem.* **2012**, *63*, 325−352.

(59) Etinski, M.; Fleig, T.; Marian, C. A. Intersystem Crossing and Characterization of Dark States in the Pyrimidine Nucleobases Uracil, Thymine, and 1-Methylthymine. *J. Phys. Chem. A* **2009**, *113*, 11809−11816.

(60) Frutos, L. M.; Andruniow, T.; Santoro, F.; Ferre, N.; Olivucci, M. Tracking the Excited-state Time Evolution of the Visual Pigment with Multiconfigurational Quantum Chemistry. *Proc. Natl. Acad. Sci. U. S. A.* **2007**, *104*, 7764−7769.

(61) Martinez-Fernandez, L.; Corral, I.; Granucci, G.; Persico, M. Competing Ultrafast Intersystem Crossing and Internal Conversion: a Time Resolved Picture for the Deactivation of 6-thioguanine. *Chem. Sci.* **2014**, *5*, 1336−1347.

(62) Richter, M.; Marquetand, P.; Gonzalez-Vazquez, J.; Sola, I.; Gonzalez, L. SHARC: ab Initio Molecular Dynamics with Surface Hopping in the Adiabatic Representation Including Arbitrary Couplings. *J. Chem. Theory Comput.* **2011**, *7*, 1253−1258.

(63) Du, L. K.; Lan, Z. G. An On-the-Fly Surface-Hopping Program JADE for Nonadiabatic Molecular Dynamics of Polyatomic Systems: Implementation and Applications. *J. Chem. Theory Comput.* **2015**, *11*, 4522−4523.

(64) Mai, S.; Marquetand, P.; Gonzalez, L. A General Method to Describe Intersystem Crossing Dynamics in Trajectory Surface Hopping. *Int. J. Quantum Chem.* **2015**, *115*, 1215−1231.

(65) Mai, S.; Richter, M.; Ruckenbauer, M.; Oppel, M.; Marquetand, P.; Gonzalez, L. SHARC: Surface Hopping Including Arbitrary Couplings-Program Package for Non-Adiabatic Dynamics. sharc-md. org.

(66) Mai, S.; Marquetand, P.; Gonzalez, L. Intersystem Crossing Pathways in the Noncanonical Nucleobase 2-Thiouracil: A Time-Dependent Picture. *J. Phys. Chem. Lett.* **2016**, *7*, 1978−1983.

(67) Weigend, F.; Haser, M. RI-MP2: First Derivatives and Global Consistency. *Theor. Chem. Acc.* **1997**, *97*, 331−340.

(68) Dunning, T. H. Gaussian-Basis Sets for Use in Correlated Molecular Calculations. I. The Atoms Boron through Neon and Hydrogen. *J. Chem. Phys.* **1989**, *90*, 1007−1023.

(69) Schirmer, J. Beyond the Random-Phase Approximation - a New Approximation Scheme for the Polarization Propagator. *Phys. Rev. A.* **1982**, *26*, 2395−2416.

(70) Sporkel, L.; Thiel, W. Adaptive Time Steps in Trajectory Surface Hopping Simulations. *J. Chem. Phys.* **2016**, *144*, 194108.

(71) Jensen, F. R.; Beck, B. H. Barrier to Inversion of 6-Membered Rings Containing an sp2-Hybridized Carbon. *J. Am. Chem. Soc.* **1968**, *90*, 1066−1067.

(72) Fournier, J.; Waegell, B. Calculation of Conformations on Stretched Systems - Pinane Derivatives. *Tetrahedron* **1970**, *26*, 3195−3219.

(73) Anet, F. A. L.; Cheng, A. K.; Krane, J. Conformations and Energy Barriers in Medium-Ring and Large-Ring Ketones - Evidence from C-13 and H-1 Nuclear Magnetic-Resonance. *J. Am. Chem. Soc.* **1973**, *95*, 7877−7878.